Quasi-analytic directional wavelet packets: applications to image processing

***Abstract*—Recently, a versatile library of quasi-analytic complex-valued wavelet packets (WPs) which originate from splines of arbitrary orders, was designed [1]. The real parts of the quasi-analytic WPs (qWPs) are the regular spline-based orthonormal WPs. The imaginary parts, which are slightly modified Hilbert transforms of the real parts, are the so-called complementary orthonormal WPs, which, unlike the symmetric regular WPs, are antisymmetric. Both regular and complementary WPs are well localized in time domain and their DFT spectra provide a variety of refined splits of the frequency domain. The waveforms can have arbitrary number of vanishing moments.**

Tensor products of 1D quasi-analytic WPs (qWPs) provide a diversity of 2D waveforms oriented in multiple directions. The designed computational scheme enables us to get fast and easy implementation of the qWP transforms. The shapes of real and imaginary parts of the qWPs can be regarded as directional cosine waves with different frequencies modulated by localized low-frequency signals. For example, the set of the fourth-level WPs comprises waveforms which are oriented in 314 different directions and are oscillating with 256 different frequencies. Various combinations of qWPs form multiple frames in the 2D signal space.

The combination of the exceptional properties of the designed qWPs, such as unlimited directionality and oscillating structure of the waveforms, vanishing moments and refined frequency resolution, make them a powerful tool for image processing applications. The algorithms based on the qWPs proved to be competitive with the best existing methods in solving such classical image processing problems as denoising, inpainting and deblurring. The qWP algorithms are especially efficient for capturing edges and fine texture and oscillating patterns even in severely degraded images.

Due to the above properties and next to unlimited diversity of testing waveforms, the qWPs have strong capabilities for extraction characteristic features from signals and images, which are utilized in the image classification algorithms in conjunction with Support Vector Machines and Convolutional Neural Networks.

I. Preliminaries

In the recent years our group has developed a toolbox which perfectly fits to signal/image processing purposes. The toolbox is based on the so-called quasi-analytic wavelet packets (qWPs), which are described in [1]. It consists of a versatile library of testing waveforms whose shapes vary from smooth well localized spline curves to fast oscillating either symmetric or antisymmetric transients. The shapes of their magnitude spectra vary from smooth bumps to near rectangular and the spectra produce a variety of refined splits of the frequency domain. The toolbox comprises very fast qWP transforms, which enable real-time processing, advanced algorithms for the signal denoising, narrow-band filtering, feature extraction and classification.

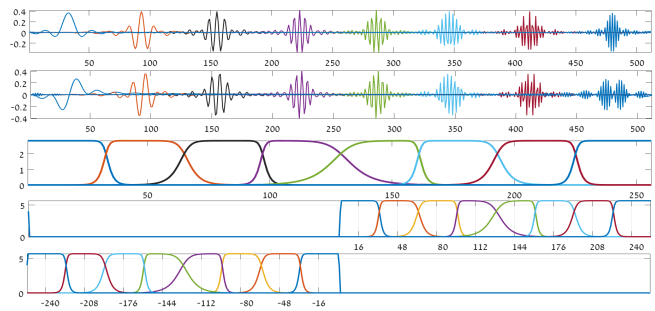

Fig. 1. Top to bottom: signals $\psi^9_{[3],l}$; signals $\varphi^9_{[3],l}$, $l = 0, ..., 7$: their magnitude DFT spectra, respectively; magnitude DFT spectra of complex qWPs $\Psi^9_{+[3],l}$; same for $\Psi^9_{-[3],l}$, $l = 0, ..., 7$

The qWPs are complex-valued signals, whose spectra occupy either the right or the left half-band of the frequency domain. The real parts of the qWPs are symmetric wavelet packets (sWPs) (Chapter 4 in [2]) originating from splines of different orders. They are denoted by $\psi^p_{[m],l}$, $l = 0, 2^m - 1$, where p is the generating spline order, m is the decomposition level and l is the index of an m-level waveform. Various combinations of shifts of the sWPs provide orthonormal bases of the signal space. The imaginary parts of the qWPs are antisymmetric. They are referred to as the complementary wavelet packets (cWPs) and denoted by $\varphi^p_{[m],l}$, $l = 0, 2^m - 1$. Their magnitude spectra coincide with the spectra of the sWPs and, similarly to the sWPs, the shifts of the cWPs provide orthonormal bases of the signal space. The cWPs are slightly modified Hilbert transforms of the sWPs. There are two families of the qWPs: $\{\Psi^p_{+[m],l} = \psi^p_{[m],l} + i\varphi^p_{[m],l}\}$, $l = 0, ..., 2^m - 1$,, whose spectra occupy the right half-band of the frequency domain and $\{\Psi^p_{-[m],l} = \psi^p_{[m],l} - i\varphi^p_{[m],l}\}$, $l = 0, ..., 2^m - 1$, whose spectra occupy the left half-band of the frequency domain.

Figure 1 displays the third-level sWPs originating from ninth-order splines; corresponding cWPs; their DFT magnitude spectra, magnitude DFT spectra of two kinds of the complex qWPs.

A standard procedure for the design of two-dimensional (2D) WPs is to compute the tensor products of 1D WPs:

$$\psi^p_{[m],\lambda,l}[k,n] = \psi^p_{[m],\lambda}[k]\, \psi^p_{[m],l}[n].$$

These 2D sWPs are separable and lack a directionality. To derive a collection of 2D WPs oriented in multiple directions, we compute the tensor products 1D qWPs:

$$\begin{aligned} \Psi^p_{+[m],\lambda,l}[k,n] &= \Psi^p_{+[m],\lambda}[k]\, \Psi^p_{+[m],l}[n], \\ \Psi^p_{-[m],\lambda,l}[k,n] &= \Psi^p_{+[m],\lambda}[k]\, \Psi^p_{-[m],l}[n] \end{aligned}$$

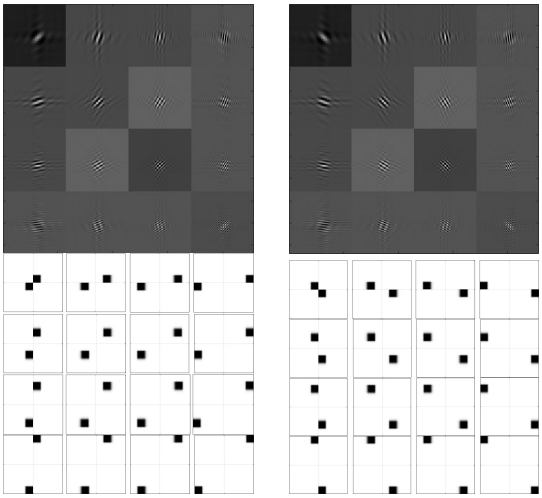

Fig. 2. Top left: WPs $\theta^9_{+[2],j,l}$ from the second decomposition; Top right: WPs $\theta^9_{-[2],j,l}$; Bottom: their magnitude spectra

level m	1	2	3	4	5	6	...
# of directions	6	22	86	314	1218	4606	...

and take real parts of these complex-valued WPs:

$$\begin{aligned}\theta^p_{\pm[m],\lambda,l}[k,n] &\stackrel{\text{def}}{=} \mathfrak{Re}(\Psi^p_{\pm[m],\lambda,l}[k,n]) \qquad (1)\\ &= \psi^p_{[m],\lambda}[k]\,\psi^p_{[m],l}[n] \mp \varphi^p_{[m],\lambda}[k]\,\varphi^p_{[m],l}[n].\end{aligned}$$

Figure 2 displays WPs $\theta^9_{\pm[2],j,l}$ from the second decomposition level and their magnitude spectra. It is seen from the figure that the 2D WPs look like windowed cosine waves which are oscillating in different directions with different frequencies. These properties stem from different dispositions and fine localization of their spectra (see [1]). Table I provides numbers of different orientations of qWPs $\left\{\vartheta^p_{\pm[m],j,l}\right\}$, $j,l = 0,...,2^m-1$, for different decomposition levels.

II. Applications

The 2D qWPs possess the following properties:

- The qWP transforms provide a variety of 2D waveforms oriented in multiple directions.
- The waveforms are close to directional cosine waves with a variety of frequencies modulated by spatially localized low-frequency 2D signals and can have any number of local vanishing moments.
- The DFT spectra of the waveforms produce a refined tiling of the frequency domain.
- Fast implementation of the transforms by using the FFT enables us to use the transforms with increased redundancy and iterative algorithms.

These properties of qWP transforms proved to be indispensable while dealing with image processing problems. Due to a variety of orientations, the qWPs capture edges even in severely degraded images and their oscillatory shapes with a variety of frequencies enable to recover fine structures. Multiple experiments on image denoising ([3]) and inpainting ([4]) demonstrate that qWP-based methods are quite competitive with the best state-of-the-art algorithms.

A. Image denoising

One of the best image denoising methods is the BM3D algorithm ([5]), which exploits the non-local self-similarity (NSS) and sparsity of images in a transform domain. This method is incomparable in restoration of moderately noised images. However, the BM3D tends to over-smooth and smear the image fine structure and edges when noise is strong. Also, the BM3D is not success when the image contains many edges oriented in multiple directions. Some improvement over BM3D was achieved by the BM3D-SAPCA [6] and WNNM [7] algorithms which rely on NSS as well. Both that methods, especially WNNM, produce state-of-the-art results in image denoising, although over-smoothing and loss some fine details while restoration of severely degraded images persists. On the other hand, algorithms that use directional oscillating waveforms provide an opportunity to capture lines, edges and texture details. Therefore, it is natural to combine the qWP-based and either BM3D [3] or WNNM [8] algorithms in order to retain strong features of both algorithms and to get rid of their drawbacks. The qWP-based denoising method (qWPdn) consists of multiscale qWP transform of the degraded image, application of adaptive localized soft thresholding to the transform coefficients using the *Bivariate Shrinkage* methodology [9], and restoration of the image from the thresholded coefficients from several decomposition levels. The combined qWPdn–WNNM method consists of several iterations of qWPdn and WNNM algorithms in a way that at each iteration, the output from one algorithm boosts the input to the other. Multiple experiments, which compared the proposed methodology with six advanced denoising algorithms, including WNNM, confirmed that the combined cross-boosting algorithm outperformed most of them in terms of both quantitative measure and visual perception. In practically all the experiments, the PSNR values for all compared algorithms are very close to each other but the SSIM values achieved by the hybrid algorithms are significantly higher than those achieved by all other algorithms. This is especially true for texture-rich images. The hybrid algorithms succeeded in restoration of the structure of even severely degraded images. It is illustrated in Fig. 3, which displays restoration of the "Mandrill" image from the input degraded by Gaussian noise with STD $\sigma = 80$ dB. The figure comprises 12 frames, which are arranged in a 4×3 order: $\begin{pmatrix} f_{11} & f_{12} & f_{13} \\ f_{21} & f_{22} & f_{23} \\ f_{31} & f_{32} & f_{33} \\ f_{41} & f_{42} & f_{43} \end{pmatrix}$. Here frame f_{11} displays noised image; frame f_{21} – image restored by BM3D; f_{12} – image restored by BM3D-SAPCA; f_{22} – image restored by WNNM; f_{13} – image restored by **Hybrid1**; f_{23} – image restored by **Hybrid2**. Frame f_{31} displays a fragment of the original image. The remaining frames $\{f_{32}, f_{33}, f_{41}, f_{42}, f_{43}\}$ display the fragments of the restored

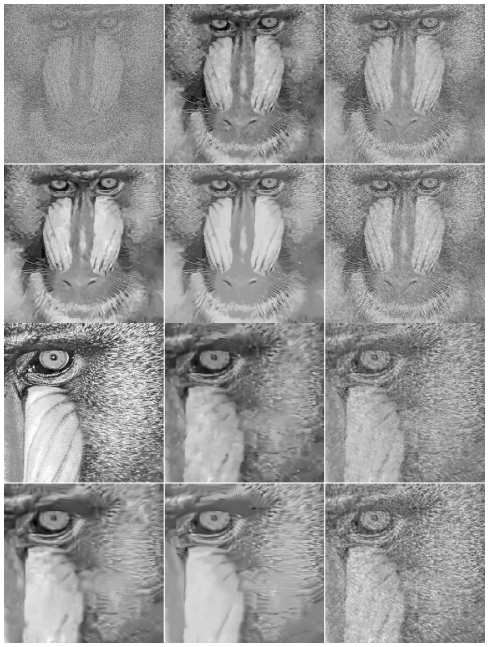

Fig. 3. Restoration of "Mandrill" image corrupted by Gaussian noise with STD $\sigma = 80$ dB. PSNR/SSIM for BM3D– 20.9/0.2439; for WNNM–21.1/0.2645; for BM3D-SAPCA–20.92/0.2649; for **Hybrid1**–20.68/0.3513; for **Hybrid2**–20.31/0.3565

images shown in frames $\{f_{12}, f_{13}, f_{21}, f_{22}, f_{23}\}$, which are arranged in the same order.

B. Image inpainting

The described qWPs demonstrated a high efficiency in dealing with the image inpainting problem, that means restoration of images degraded by the loss of a significant share of pixels and possible addition of noise. We designed a qWP-based iterative algorithm, which combines the split Bregman iteration scheme ([10]) with the adaptive decreasing thresholding ([11]). In multiple experiments on restoration of images corrupted by missing a large amount of pixels and addition of Gaussian noise with various intensities, we compared the performance of our qWP-based algorithm with the performance of a number of the state-of-the-art algorithms. The description of the algorithm and results of from multiple experiments on image inpainting are presented in the paper [4]. Similarly to denoising experiments, the qWP algorithm **QA** prevailed in restoration of edges and fine structure even in severely degraded images. This fact is reflected in highest values of SSIM. This method succeeds in capturing fine details in the images in cases where other state-of-the-art algorithms fail. This fact is illustrated in Fig. 4, which displays the restoration results of the 'Mandrill" image from the input where 80% of pixels are missing and additive Gaussian noise with $\sigma = 50$ dB is present. The output from the DAS-2 algorithm ([12]) (which is one of the best in the field) has PSNR=19.81 dB compared to 18.93 dB produced by **QA**. On the other hand, the SSIM from the **QA** restoration is 0.2343 compared to 0.1414

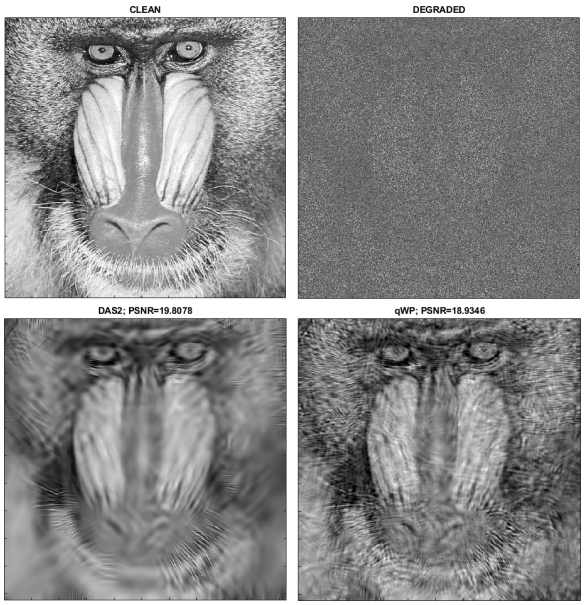

Fig. 4. Restoration of the "Mandrill" image. Top left: clean image. Top right: image degraded by loss of 80% of pixels and additive Gaussian noise with $\sigma = 50$ dB. Bottom right: **QA** restoration, PSNR=18.93 dB, SSIM=0.2343. Bottom left: DAS-2 restoration, PSNR=19.81 dB, SSIM=0.1414

produced by DAS-2. We can see that many texture patterns that were blurred by DAS-2, are restored by **QA**.

C. Image classification

A key point in image classification is the extraction of a limited number of features that characterize single images and sets of images to be classified. We claim that due to the exceptional properties of the directional qWPs they can serve as a perfect tool for that purpose. Such characteristic pattern in images as edges and texture patches oriented in different directions are successfully captured by qWPs. Most important is the fact that the extracted features have a clear physical meaning. Namely, the features are correlation coefficients of fragments of the image with certain qWP waveforms. This is illustrated in Fig. 5.

We conducted a few experiments with the MNIST database of handwritten digits to test feasibility of the qWP-based feature extraction scheme for the image classification. The MNIST database contains 60,000 training images and 10,000 testing images. We explored two options of the qWPs' utilization:

1) Extraction of qWP-based characteristic features from limited numbers of training images and using them for training the Support Vector Machine (SVM, [13]) classifier. Then, the trained SVM was used for the classification of 10,000 testing images. Preliminary results of the experiments confirmed efficiency of such a scheme even with small reference datasets used for training SVM.
2) Convolutional Neural Networks (CNNs) achieve extraordinary success in image classification. The convolution

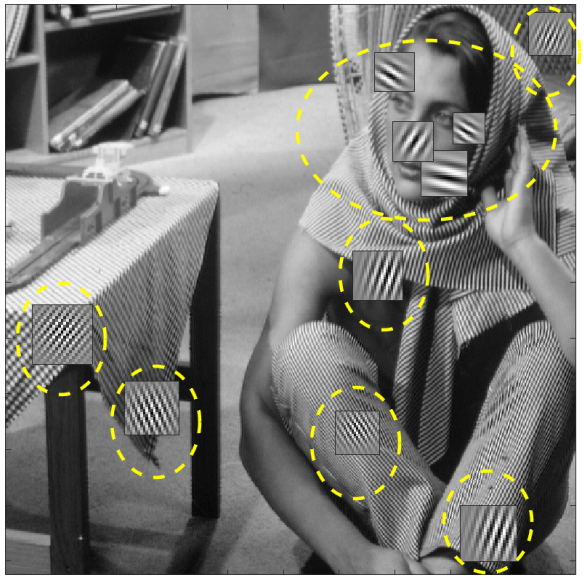

Fig. 5. Illustration of physical meaning of feature extraction by qWPs

Size of ref. set	60000	20000	10000	5000	2000	1000	500	300
SVM class%	98.42	98.61	98.2	97.76	97.32	96.49	94.53	94.19
CNN class%	99.51	99.18	98.79	98.26	97.38	96.08	94.12	92.67

TABLE I
CLASSIFICATION RESULTS FOR THE VALIDATION SET OF 10,000 IMAGES

layers in a CNN extract the characteristic features from the training data by convolving the input data with filters that are derived in the training process. Consequently, the structure of the filters and the meaning of the extracted features remain unclear. Such a scheme requires a huge amount of data and a large number of convolution layers. Thus, it is natural to replace at least some of the convolution layers in the CNN by filtering with predefined filters whose properties are favourable to the class of images under processing. This is done in our second series of the experiments where absolute values of the qWP transform coefficients serve as the inputs to a CNN with a small number of convolution layers. Recall that the qWP transform coefficients have a clear physical meaning.

Some results, which are given in Table I, indicate that the qWP-based feature extraction methods have a potential to handle image classification problems. The table shows percentage of correct answers from the SVM classifiers and the CNNs, which are trained on reference sets comprising different numbers of images, for the validation set comprising of 10,000 images.

Note that in the cases when the training database is small, the classification results from SVM prevail over those from CNN and vice versa for the big databases.

III. CONCLUSION

The designed directional qWPs provide powerful tools for solving various signal and image processing problems. A vast diversity of the directional oscillating waveforms enables extraction of characteristic features with clear physical meaning from images. The current field of our research is coupling those feature extraction capabilities with Deep Learning methods. Our first experiments with MNIST and CIFAR10 image databases reveal a strong potential of such a combination.

ACKNOWLEDGMENT

This research was partially supported by the Israel Science Foundation (ISF, 1556/17, 1873/21), Israel Ministry of Science Technology and Space 3-16414, 3-14481.

REFERENCES

[1] Anonimous.
[2] ——.
[3] ——.
[4] ——.
[5] K. Dabov, A. Foi, V. Katkovnik, and K. Egiazarian, "Image denoising by sparse 3d transform-domain collaborative filtering," *IEEE Trans. Image Process.*, vol. 16, no. 8, pp. 2080—-2095, 2007.
[6] ——, "BM3D image denoising with shape adaptive principal component analysis," in *Proceedings of the Workshop on Signal Processing with Adaptive Sparse Structured Representations (SPARS'09)*, 2009.
[7] S. Gu, L. Zhang, W. Zuo, and X. Feng, "Weighted nuclear norm minimization with application to image denoising," in *2014 IEEE Conference on Computer Vision and Pattern Recognition*, 2014, pp. 2862–2869.
[8] Anonimous.
[9] L. Şendur and I. W. Selesnick, "Bivariate shrinkage functions for wavelet-based denoising exploiting interscale dependency," *IEEE Trans. Signal Process.*, vol. 50, pp. 2744–2756, 2002.
[10] T. Goldstein and S. Osher, "The split Bregman method for $L1$-regularized problems," *SIAM J. Imaging Sci.*, vol. 2, no. 2, pp. 323–343, 2009.
[11] Y. Shen, B. Han, and E. Braverman, "Image inpainting from partial noisy data by directional complex tight framelets," *Anziam J.*, vol. 58, no. 3–4, pp. 1–9, 2017.
[12] Z. Che and X. Zhuang, "Digital affine shear filter banks with 2-layer structure and their applications in image processing," *IEEE Trans. on Image Processing*, vol. 27, no. 8, pp. 3931–3941, 2018.
[13] A. Ben-Hur, D. Horn, H. Siegelmann, and V. Vapnik, "Support vector clustering," *Journal of Machine Learning Research*, vol. 2, pp. 125–137, 2001.